Disparity increment thresholds for gratings

Bart Farell Institute for Sensory Research, Syracuse University Syracuse, NY, USA

Simone Li Institute for Sensory Research, Syracuse University Syracuse, NY, USA

Suzanne P. McKee Smith-Kettlewell Eye Research Institute San Francisco, CA, USA

The classic increment disparity threshold function rises steeply, usually exponentially, with disparity pedestal. Thus a smaller difference in stereoscopic depth can be resolved the nearer it is to the fixation plane. This result has been obtained with relatively broad-bandwidth stimuli. We show here that the increment threshold function for narrow-bandwidth stimuli differs subtly from the classic function: Thresholds vary only modestly over a ± quarter-cycle pedestal range, by a factor of about 2, and frequently show a dip, yielding best stereo acuity not at the fixation plane but at moderate disparities (20°- 30° in phase) on either side of it. Though the dip has not been noted previously, it is consistent with models of disparity processing in which filter sensitivity or selectivity is greatest at a disparity of zero. Moreover, the relatively flat increment threshold function observed at any one scale is compatible with a steeply rising function for broad-bandwidth stimuli.

Keywords: stereo vision, depth perception, stereo acuity, binocular disparity, increment thresholds

Introduction

Two objects separated in depth produce retinal images with disparities P and $P + I$. Fixating on or near the plane of one object makes P, the pedestal disparity, small. It is when the pedestal is small that the depths of the objects are most discriminable: Threshold for detecting the disparity increment I rises, usually exponentially, with increases in P (Ogle, 1953; Blakemore, 1970; Regan & Beverley, 1973; Krekling, 1974; Westheimer & McKee, 1978; Westheimer, 1979; Schumer & Julesz, 1984; Badcock & Schor, 1985; McKee, Levi, & Bowne, 1990; Andrews, Glennerster, & Parker, 2001). Only near the horopter is sensitivity to relative disparity I found to be within the hyperacuity range (Westheimer, 1979). Thus sensitivity to relative disparity depends on the absolute disparity, and so varies with P, even though sensitivity to absolute disparity per se is notoriously poor (Westheimer, 1979; Erkelens & Collwijn, 1985; Regan, Erkelens, & Collwijn, 1986).

What causes disparity discrimination to deteriorate as the stimulus is placed further from the fixation plane? The answer may depend on the stimulus. For a stimulus with a broad spatial-frequency bandwidth, the discrimination threshold measured at one disparity pedestal may be based on different frequency components than the threshold measured at another pedestal. High-frequency components of the stimulus would limit threshold at small pedestals and low-frequency components would do so at large pedestals. The increment threshold function, like the stimulus, would be a composite. One can model the rising disparity increment threshold function by increasing the bandwidth of disparity tuning with preferred disparity, as Lehky and Sejnowski (1990) did. But whether such a bandwidth increase should be understood as a by-product of a shift to lower-frequency components cannot be resolved by data from previous studies; the stimuli used were too broadband to reveal the shape of the increment threshold function for a single scale. Here we use grating stimuli with narrow spatial-frequency and orientation bandwidths and present them at low contrast. These stimuli limit the range of disparities over which fusion and monotonic variation in perceived depth occur; their advantage is that they engage a correspondingly restricted range of mechanisms. The increment thresholds we measure for these single-scale stimuli do not fit the mold of the classic increment threshold function and provide clues about the organization of disparity mechanisms.

Increment thresholds and the size-disparity correlation

Increment thresholds have the potential for revealing channel disparity tuning. This is clearest in cases where disparity-processing channels are few in number and broadly tuned (e.g., "near" vs. "far") (Richards, 1971). For tuning functions whose slope varies inversely with disparity (e.g., Poggio & Fischer, 1977), large response changes would arise from small disparity changes near the plane of fixation; this is where discrimination would be best. Discriminating large disparities would be possible only if their difference is big enough to overcome the low responsivity gain. Thus increment thresholds would increase with ped-

doi:10.1167/4.3.3 Received March 4, 2003; published March 16, 2004 ISSN 1534-7362

estal disparity, following the inverse of the derivative of the tuning function.

A multi-scale analysis of disparity would complicate this picture. Multi-scale processing links disparity tuning and resolution largely through the size-disparity correlation (Felton, Richards, & Smith, 1972; Marr & Poggio, 1979; Schor & Wood, 1983; Schor, Wood, & Ogawa, 1984a; Smallman & MacLeod, 1994; Harris, McKee, & Smallman, 1997). By this correlation, fine-scale channels limit discrimination thresholds at small disparity pedestals and coarse-scale channels do so at large disparity pedestals. Coupled with scale-dependent resolution, this provides for Weber-law discriminability, with low-frequency mechanisms providing for low-resolution disparity discrimination over a broad range of disparities and high-frequency mechanisms providing for higher-resolution disparity discrimination over a narrower, near-horopter range (Qian & Zhu, 1997; Smallman & MacLeod, 1997; Tsai & Victor, 2003). The size-disparity correlation is built into phase-offset coding of binocular disparity (Ohzawa, DeAngelis, & Freeman, 1990; Fleet, Jepson, & Jenkin, 1991; Fleet, Wagner, & Heeger, 1996) and also arises from a parsimonious implementation of spatial-offset coding.

Thus each mechanism has a scale-dependent disparity range and resolution. So, a stimulus whose spatial-frequency bandwidth is broad relative to that of individual channels is unlikely to produce a disparity increment threshold function that depends on any one channel. Not only spatial-frequency bandwidth but also orientation bandwidth and contrast must be taken into account in evaluating channel contributions to the increment threshold function — orientation, because a broader range of horizontal disparities can be read by an obliquely oriented receptive field than by a vertical one; and contrast, because a wider range of spatial-frequency and orientation components can contribute to disparity detection at high than at low contrast. Among the band-limited patterns previously used to measure increment thresholds, Rohaly and Wilson's (1993) D6 patterns had a full-width, half-amplitude spatial-frequency bandwidth of one octave and a contrast of 50%, whereas Badcock and Schor's (1985) difference-of-Gaussians had a spatial-frequency bandwidth of 1.75 octaves and a contrast of 100%. Differences-of-Gaussians with this bandwidth were also used by Siderov and Harwerth (1993a, 1993b), though generally at a lower contrast. McKee, Levi, and Bowne (1990) used high-contrast lines as stimuli. All these patterns were oriented and their orientation bandwidths varied from one to another. Spatial-frequency bandwidths varied inversely with center frequency in Smallman & MacLeod's (1997) filtered random-dot stereograms (RDSs), which had a root mean square (RMS) contrast of 0.3, but these RDSs were isotropically filtered, so the stimulus horizontal spatial-frequency bandwidth was larger than the filter bandwidth. Schumer and Julesz (1984) used unfiltered RDSs and varied the frequency of the disparity modulation. Only in these studies using RDSs was disparity generated by offsetting just the carrier rather than by offsetting both the carrier and the envelope; an envelope offset may introduce monocular cues (Smallman & MacLeod, 1997; McKee, Levi, & Bowne, 1990) and second-order matching (Hess & Wilcox, 1994; Schor, Edwards, & Pope, 1998; Langley, Fleet, & Hibbard, 1999, McKee, Verghese, & Farell, in press; Stelmach & Buckthought, 2003).

We measured thresholds for discriminating interocular carrier phase shifts of grating patches with relatively narrow spatial-frequency and orientation bandwidths and relatively low contrasts in order to avoid multi-channel responses and interactions. For comparision, we also measured thresholds for unfiltered RDSs. Initially the stimuli were presented in two-interval forced-choice trials, with the stimulus appearing at the pedestal disparity in one interval and at the pedestal-plus-increment disparity in the other. We also measured increment thresholds using several other versions of the task, each with two or three observers. This allowed us to gauge the generality of the results and assess the influence of potential artifacts specific to particular methods.

Methods

Stimuli

Gratings were sinusoidal luminance modulations limited spatially by either hard-edged or Gaussian circular envelopes; in one condition, a wide cosine envelope was also used. The gratings' orientation was vertical (90°) and their contrast was 0.1 in most conditions; the other values investigated were 30° in orientation and 0.2 in contrast. Most data were collected at spatial frequencies of 0.5, 1.0, and 2.0 c/d; in other conditions, spatial frequency ranged between 0.33 and 6.0 c/d. Stimuli were generally presented for durations of 150 ms and separated in time by 0.5 s in two-interval methods.

The hard-edged envelope was 8° in horizontal and vertical extent for all spatial frequencies. The Gaussian envelope had a standard deviation of $\sigma = \sqrt{2}/f°$ for spatial frequency f and was truncated at $\pm 2\sqrt{2}\sigma$. The spatial-frequency bandwidth of these Gabor patches, measured at half height and full width, was 0.38 octaves. RDSs were made of 2 min square checks with a Gaussian luminance distribution with a RMS contrast of 0.3; RDS displays were square, hard-edged, and 1.4° on a side. In all cases but one, the screen beyond the stimulus boundaries had a uniform luminance of approximately 20 cd/m^2, equal to the mean stimulus luminance. (The exception, at 65 cd/m^2, was for one condition run in a second lab on different equipment, as described in the caption of Figure 2.)

This exceptional condition aside, left and right half-stimuli were displayed on the two sides of a luminance-calibrated CRT and viewed through a mirror stereoscope. For gratings, the visible screen subtended approximately 10.5° (horizontal) × 16° (vertical) in visual angle; for RDSs, screen resolution was increased by a factor of 2.4 and view-

ing distance by a factor of either 2 or 4, to accommodate individual observer's thresholds. The stimulus envelope was centered on black fixation squares, either 6 min or 3 min of visual angle on a side, which were continuously visible throughout the run of trials. In all cases, the envelope had a disparity of zero. The only nonzero disparities were interocular carrier phase shifts.

Two computer programs were used. One was written in C and controlled the three guns of the monitor operating with a frame rate of 120 Hz. Alternate frames presented the stimulus to left and right eyes. Each half-stereogram was drawn using separate color lookup tables to achieve subpixel resolution. The other program was written in MATLAB using the Psychophysical Toolbox extensions (Brainard, 1997; Pelli, 1997) and employed an attenuator (Pelli & Zhang, 1991) to combine the video outputs to drive the monitor's green gun with a luminance resolution of about 12 bits; the frame rate was 75 Hz, with each frame presenting the stimulus to both eyes. Disparity in the first program was produced by shifting the phase of the grating presented to one eye and in the second program by shifting the phase of both gratings by equal and opposite amounts. No systematic difference appeared between data collected by the two programs. Pixel-unit (0.16 min or 0.32 min) shifts to either one or both half-stereograms were used for RDSs; as with grating envelopes, the disparity of the RDS envelope was fixed at zero.

Procedure

A number of methods were used. They differed in whether they required discrimination of increments and decrements or pedestal-plus-increments and pedestal-plus-decrements, whether they required discrimination of disparity sign or magnitude, whether they were susceptible to fixation disparities, and whether, and by how much, they relied on memory of disparities presented in previous intervals or previous trials. The methods were similar in that a difference in carrier disparity was the signal in all cases.

In the two-interval methods, the stimuli were identical across the two intervals except for the disparity and absolute phase of the gratings. In one interval, the grating had the pedestal disparity, and in the other, the pedestal disparity plus an increment. In separate conditions this increment was always positive and required a two-interval forced-choice detection (Figure 1a), or was either positive or negative and required a "Near"/"Far" forced-choice discrimination (Figure 1b) (Farell, 1998). The absolute phases of the gratings were randomized in every interval identically for the two eyes, translating the grating unpredictably between intervals, eliminating possible positional cues without affecting disparity.

Two single-interval methods were used. In one, the stimulus was a bipartite Gabor patch — two half-Gabor patches separated by a hard-edged horizontal band 18 min high (Figure 1c). The lower patch was presented at the pedestal disparity. The upper patch was presented either at the pedestal-plus-increment disparity or at the pedestal-plus-decrement disparity, where increments and decrements were equal in absolute value. The observer judged the upper patch as "Near" or "Far" relative to the lower patch.

The second single-interval task was a form of absolute identification using the method of single stimuli. There were two versions. In the two-pedestal version, illustrated in Figure 1d, a grating was presented on each trial at one of four alternative disparities. These disparities were the combinations of two pedestals, one positive and one negative (gray disks in Figure 1d), and two increments, one positive and one negative. The absolute magnitudes of the two pedestals were the same, as were the absolute magnitudes of the two increments. The observer's task was to classify the grating with respect to its distance from the fixation point; two of the grating positions were "Near" the fixation point and two were "Far." At a pedestal of zero, the two pedestals were no longer distinct and the task simplified to a discrimination between just two alternative grating positions, one on either side of the fixation plane. In the one-pedestal version, only the positive pedestal was used and the disparity of the grating varied from trial to trial. Performance in the nonzero-pedestal conditions of these tasks, unlike the other tasks, depends on memory across trials; indeed, the first trial of a run contains no information on which to base a response. Hence, for this method only, feedback about the correctness of responses was provided, as were practice trials within each run before data-collection trials began.

Except for the absolute-identification tasks, trial-to-trial disparities were under the control of the QUEST algorithm (Watson & Pelli, 1983; King-Smith et al., 1994) with a threshold criterion of 82% correct. A constant-stimulus method was used for the two-pedestal absolute-identification task, where psychometric functions were fit with a Weibull function and the disparity yielding 67% correct responses was taken as threshold (the task was difficult and two of the four observers did not reach even this level of performance). The one-pedestal version used QUEST for one observer and constant stimuli for the other, with 82% and 75% threshold criteria, respectively.

Responses were made by clicking a mouse. A subsequent click initiated the following trial.

Data were collected in runs of 40-80 trials, depending on the method, and observers typically had 4-5 runs per condition. Threshold statistics (means and SEs) were based on one estimate per run.

In principle, periodic stimuli have a useful phase-disparity range spanning ±180°. In practice, this range encompasses several qualitatively distinct percepts (Ogle, 1952; Tyler, 1991), and this makes the measurement of thresholds on large pedestals problematic (see Badcock & Schor, 1985; Siderov & Harwerth, 1993b). Gratings with phase disparities much more than 90° often appeared diplopic (consistent with the results of other studies; e.g., Schor, Wood, & Ogawa, 1984b), or with ambiguous or

reversed depth at disparities well below 180°. These variations in the percept could cause the observer's task to change as the pedestal disparity varies. For example, an increment in disparity that is discriminated by a quantitative change in perceived depth at a small pedestal might be discriminated by a qualitative change in the percept (fusion vs. diplopia, or appropriate depth polarity vs. reversed depth polarity) at a large pedestal. Near the transition point, the increment threshold function can become nonmonotonic (see description of the vertical disparity threshold function in Discussion). Our interest here is in increment thresholds mediated by changes in perceived depth, so pedestals were limited to phase offsets of 90° or 120°, keeping the disparity (pedestal plus increment) below the diplopia, depth-ambiguity, and depth-reversal thresholds.

Observers

Five observers, four of them (including two of the authors) highly experienced in stereo experiments, were run in the experiments. Not all observers ran in all four of the methods. Two of the observers were naïve about the purposes of the experiments. All had normal or corrected-to-normal acuity and normal stereo vision.

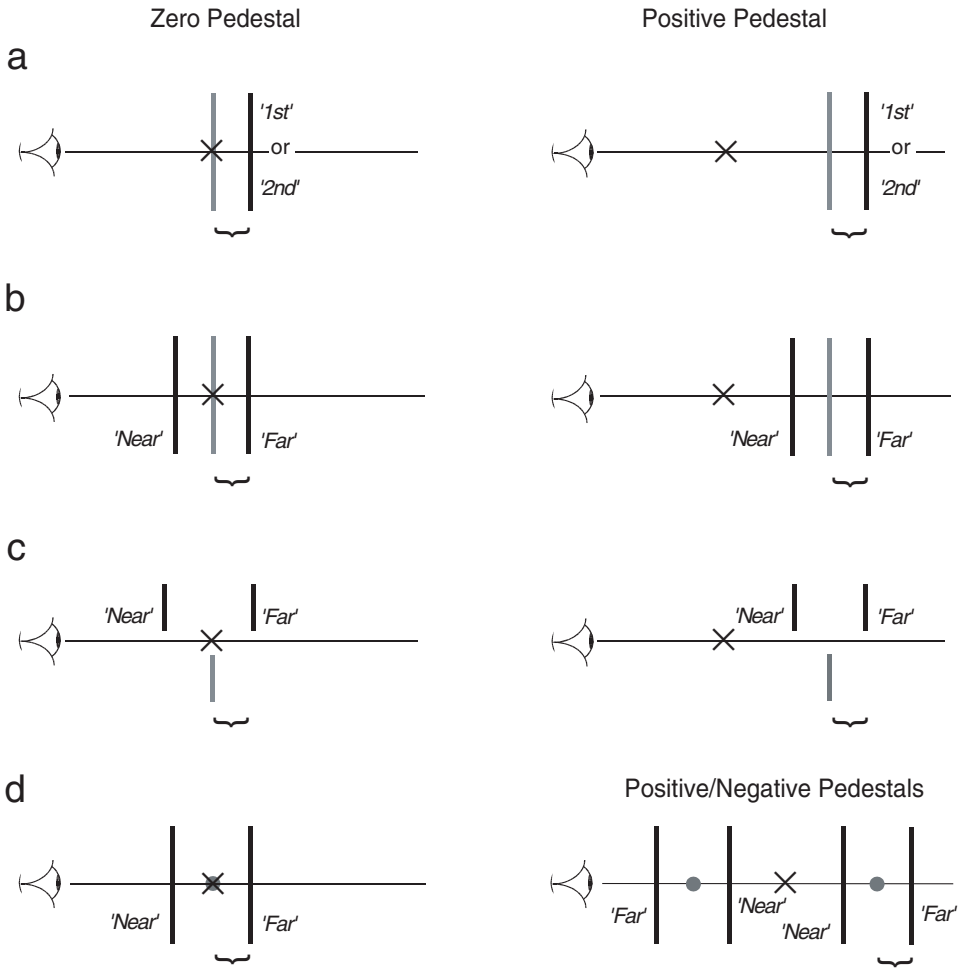

Figure 1. Four methods of measuring disparity increment thresholds. The left side shows stimulus configurations presented with a pedestal disparity of zero; the right side shows configurations with nonzero pedestal. a. Two-interval detection. The observer chooses the interval in which the grating appears with pedestal-plus-increment disparity. b. Two-interval discrimination. The observer judges the depth of the grating ("near" vs. "far") shown in the second interval relative to that of the pedestal-disparity grating shown in the first interval. c. Single-interval discrimination. The observer judges the depth of the upper grating relative to the pedestal-disparity lower grating. d. Absolute identification, method of single stimuli. The observer judges the grating's disparity magnitude relative to the fixation marker. In this method, the four alternative positions in depth arrayed around nonzero pedestals (right) reduce to two when the pedestal is zero (left). In d, the pedestals are marked by disks. For all cases, light bars are at the pedestal disparity, dark bars are at the pedestal plus or minus a disparity increment, and the curly bracket shows the disparity increment. A fixation point was present throughout the run of trials in all conditions. For two of the observers, nonius lines were presented above and below the fixation point; these disappeared 125 ms before stimulus onset and returned after the observer responded. The importance of maintaining fixation throughout stimulus presentations was stressed.

Results

The disparity increment thresholds shown in Figures 2a and 2b were collected using the two-interval methods, and those shown in Figures 2c and 2d are from the one-interval methods. For two of the three observers tested with both pedestal polarities, thresholds were approximately symmetrical about the fixation plane, showing essentially equivalent results for positive and negative pedestals. One observer showed higher thresholds for negative pedestals, by nearly a factor of 2. Where applicable, data for increments and decrements were combined and thresholds examined as a function of the pedestal's absolute value.

A typical dataset is shown in Figure 2a, where thresholds and pedestal disparities for 1 c/d gratings are expressed as phase offsets (in degrees) and as spatial dis-

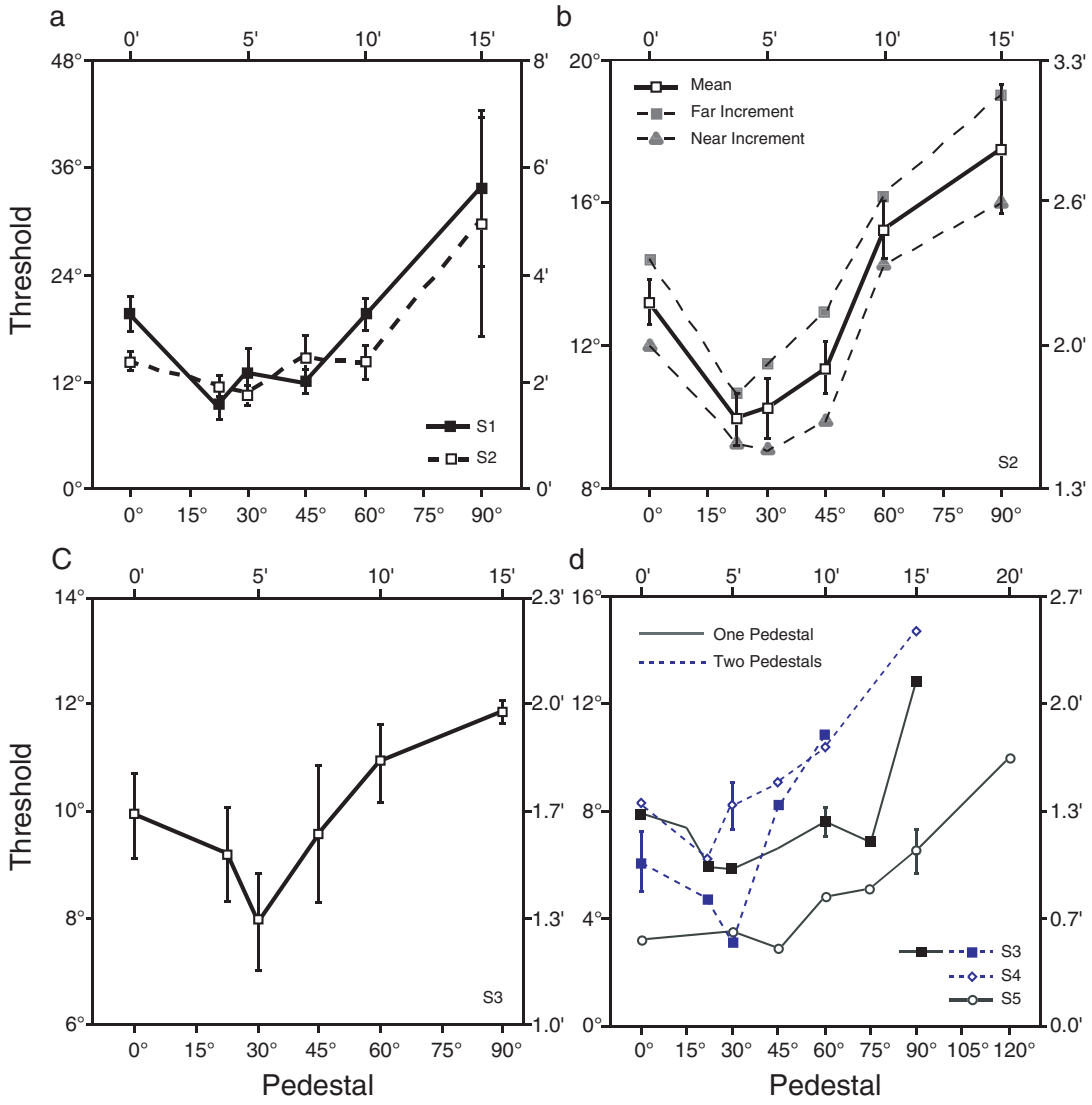

Figure 2. Disparity increment thresholds as a function of disparity pedestal for vertical 1 c/d gratings with contrast of 0.1. Pedestal disparities (abscissa) and threshold disparities (ordinate) are given as degrees of phase (bottom and left scales) and as minutes of visual angle (top and right). a. Grating had a hard-edged envelope 8° in diameter. Two observers' data are shown. The method was two-interval detection (Figure 1a). b. Thresholds for the same stimulus as in a, using the two-interval discrimination method (Figure 1b). Data for near and far increments and their means are plotted. c. Thresholds for a bipartite Gabor patch using the single-interval discrimination method (Figure 1c). d. Blue symbols connected with broken lines show thresholds for the hard-edged grating, as in a, measured with the two-pedestal absolute-identification method (Figure 1d); threshold criterion was 67% correct, rather than the default 82%. Black symbols connected with solid lines show thresholds for a Gabor patch (S3) or 8°-wide cosine-windowed grating (S5) measured with the one-pedestal absolute-identification method. Vertically the cosine-windowed grating was hard edged and 2° in extent; it was presented for 200 ms on separate monitors for left and right eyes, with mean screen luminance of 65 cd/m^2; threshold criterion was 75%. The fixation plane was marked by a short bar at the same contrast as the stimulus and located below it. Note that the ordinate is scaled differently across the four graphs. Error bars are ±1 SEM; single bars give the condition average.

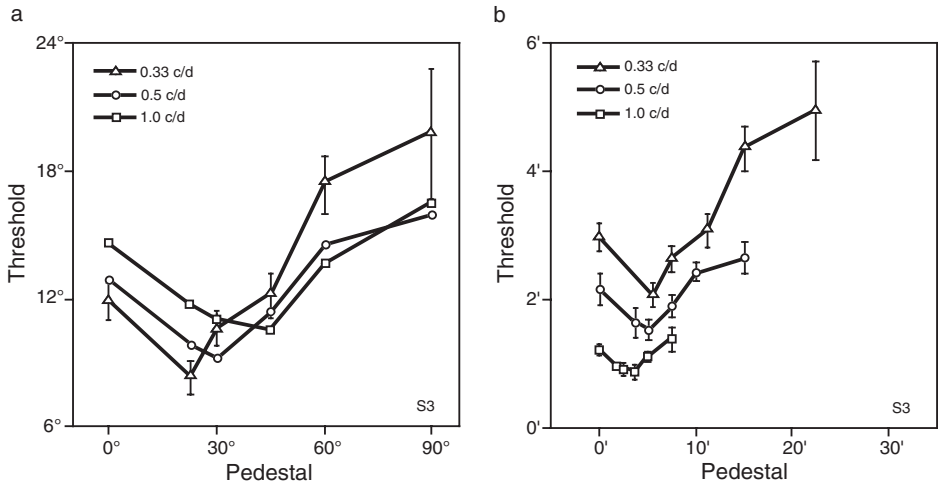

Figure 3. Disparity increment thresholds for gratings of different frequencies using the two-interval detection method (Figure 1a). a. Phase disparity thresholds for gratings with spatial frequencies of 0.67, 1.0, and 2.0 c/d plotted as a function of pedestal size. Despite considerable phase disparity constancy, there is a marginal shift of the low pedestal thresholds upward and the high pedestal threshold downward as frequency increases, displacing the dip to larger pedestals. For clarity, error bars (±1 SEM) are shown for only one frequency. b. Data of panel a plotted as spatial threshold in units of minutes of visual angle. The location of the dip is invariant in neither spatial nor phase disparity.

placements (in minutes of visual angle) for two observers. The data come from the two-interval increment detection method (Figure 1a). The noticeable dip and the roughly 2:1 range of thresholds across the 0°-90° range of pedestal values was also found using the two-interval increment discrimination method (Figure 1b) and the single-interval bipartite-stimulus method (Figure 1c), as seen in Figures 2b and 2c, respectively. Thresholds for the two-pedestal absolute-identification method (Figure 2d) were unmeasurable for two observers tested and required a reduced criterion for threshold (67% correct) for the two who could perform the task. Even with the low criterion, threshold could be measured on only one observer at the largest pedestals (90°). The psychometric functions on which thresholds were based were shallow, noisy, and asymptoted at low values.[1] Yet thresholds were low and resembled those obtained by other methods in showing a dip followed at larger pedestal sizes by a rise in threshold.

In general, and for all the methods, grating thresholds were little higher at a pedestal phase disparity of 60° than at 0°, but then show a larger increase at 90°. Across a pedestal phase disparity range of 0° to 90°, increment thresholds typically occupy a 2- to 3-fold range of values overall. The fine structure shows a dip for most observers, with the lowest thresholds occurring at a pedestal of approximately 30°. There was little systematic effect of spatial frequency on threshold phase disparity over the 0.33–6.0 c/d range tested, though threshold phase angles were somewhat elevated for frequencies greater than 2 or 3 c/d, as is generally observed (Schor & Wood, 1983; Legge & Gu, 1989). Also, no systematic difference in phase disparity thresholds appeared between gratings with different orientations (30° and 90°) (for the effect of orientation on disparity thresholds, see Farell, 2003). Likewise, there was no systematic effect of grating envelope type, hard-edged or soft.

The scaling of increment thresholds with spatial frequency is shown in Figure 3 for the two-interval detection method (Figure 1a). Thresholds are plotted as phase offsets in Figure 3a and spatial offsets in Figure 3b. For these low-to-moderate frequencies, threshold scales approximately with frequency, showing rather greater constancy when plotted as phase disparity than as spatial disparity. However, the location of the dip is not invariant; it shifts to somewhat larger phase-disparity pedestals, and somewhat smaller spatial-disparity pedestals, as frequency increases.

Increment thresholds for random-dot displays appear in Figure 4. The two-interval detection method (Figure 1a) was used. There is no dip. Exponential functions provide an excellent fit to the data points ($r = 0.997$ for observer S3 and $r = 0.989$ for observer S1 vs. 0.954 and 0.961, respectively, for the best-fitting linear functions).

Discussion

The detection of disparity increments has been characterized by two main features: Thresholds are smallest near the fixation plane, and they increase, usually exponentially, as the pedestal extends in depth in either direction from this plane. While both of these classic features apply to our data for random-dot stereograms, new features characterize our data for narrow-band grating patches at pedestal phase disparities within the range of about $\pm\pi/3$. In our study, increment thresholds for grating patches rose sharply above the value observed at zero pedestal, but typically only after the pedestal was large (>60° phase), roughly half or more of the diplopia threshold. At smaller pedestals, thresholds

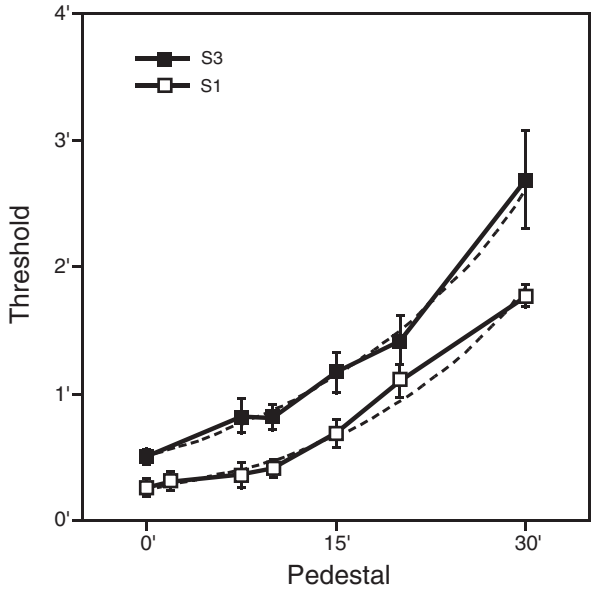

Figure 4. Disparity thresholds for random-dot stereograms as function of disparity pedestal for two observers. The method was two-interval detection. The dotted line shows the best-fitting exponential function. Error bars are ±1 SEM.

were confined to a rather narrow range within which variation was typically nonmonotonic; there was a dip.

In principle, a fixation disparity could account for both the dip and the small threshold range in some of the datasets, but not in all of them. If the true increment threshold function is monotonic, the observed threshold minimum would be at zero pedestal. But a consistent fixation disparity could put the minimum at a nonzero pedestal value corresponding to the observer's actual fixation plane. And when the set of alternative pedestal values for each trial is not symmetrically distributed about the nominal fixation plane, a fixation disparity could also make the effective pedestal smaller in absolute value, thereby lowering thresholds. The bipartite Gabor stimulus is susceptible to both of these artifacts. However, the two-interval stimulus presentations should be immune to them. This is because a fixation disparity leaves the depth interval that the observer judges — the depth interval between fixation point and grating (Westheimer, 1979) — unchanged. The same applies to the absolute-identification tasks. The two-pedestal version, with stimuli symmetrically arrayed about the fixation point, seems to allow no strategy that would impart an advantageous fixation disparity; vergence changes that bring positive-disparity stimuli closer to fixation move negative-disparity stimuli farther away. Because the dip and modest threshold range are common to the results of all the methods used, they would appear to be real features of the increment threshold function for the grating stimuli used here. Indeed, the differences between the tasks — in the depth intervals to be discriminated, the requirement of discriminating disparity sign or magnitude, and the disparity memory required for the discrimination — had rather little effect on the data.

One may ask, though, about the extent to which the stimuli determined the results, independent of computational algorithm or architecture. For a periodic stimulus, disparity is ambiguous; adding an integer multiple of its period to its nominal disparity leaves the stimulus unchanged. If the stimulus is subject to a nearest-neighbor matching constraint or a minimal disparity constraint, then its phase-disparity is confined to a range of ±180°. At disparities of ±180°, the left and right images are anticorrelated. At a disparity of zero, their correlation is 1.0. At disparities of ±90°, the correlation between the left and right images is zero, and it is at this disparity that the slope of the correlation function is at its maximum. Therefore, if disparity increments are detected as changes in interocular correlation, sensitivity to disparity increments would be expected to be highest about disparities of ±90°. However, there is no evidence in the increment threshold function for a dip, or any other performance advantage, at or around a disparity pedestal of 90°. Instead, the threshold minimum is found typically around 30°.

One can suppose that the dip found at a pedestal of about 30° is only a vestige of the larger dip centered at 90° predicted by this correlational process. There could be an additional process that unlike correlation depends only on disparity and drives the thresholds of all stimuli up equally, and perhaps exponentially, at large pedestals. It could be the source of the exponential increase usually seen in disparity increment thresholds, as in the RDS data of Figure 4. This increase might have swamped most of the 90° dip in the grating threshold function, leaving only the initial part of this dip, centered around 30°. Indeed, the dip shifts toward larger phase angles as grating frequency increases (Figure 3), which is consistent qualitatively with such a two-process account, though quantitatively it is a smaller shift than predicted. However, thresholds for different frequencies show no sign of converging at large pedestal values, as the two-process notion requires. Elsewhere we argue, contrary to this two-process explanation, that thresholds for single-scale components shape the threshold function for multi-scale stimuli such as RDSs and account for their relatively low threshold values (Farell, Li, & McKee, in press).

One can find in the literature several studies that hint at nonmonotonicities suggestive of a disparity dipper, and two studies in which the dipper is full-blown. The latter are the studies of Duwaer and van den Brink (1982) and McKee, Levi, and Bowne (1990), where the disparities giving rise to the dip were *vertical*. Using horizontal lines, Duwaer and van den Brink found that thresholds for discriminating vertical disparities dropped by roughly a factor of 2 as the pedestal increased from zero, before rising again. Thresholds were minimal at pedestals ranging from 2.4 min to 15.3 min, depending on line length, eccentricity, and presentation duration. Similarly, minimal thresholds for horizontal lines in the McKee, Levi, and Bowne (1990)

study occurred at pedestals of about 15 min. In studies of horizontal disparity thresholds, nonmonotonicities appear faintly in the data of Smallman and MacLeod (1997), whose filtered RDSs were tested at quite large pedestal phase disparities but not at zero, and possibly in those of Siderov and Harwerth (1993a, 1995), who used difference-of-Gaussian patterns.

Accounting for the dip

Duwaer and van den Brink (1982) interpreted the dip in vertical disparity thresholds as evidence for two near-horopter processes: loss of sign and increased noise. Either process alone would be sufficient to generate a dip in disparity discrimination thresholds, provided that disparity resolution decreases away from the horopter. By itself, however, a loss of sign would not affect detection thresholds. At zero pedestal, the detection task used here requires only a discrimination of disparity magnitude, whereas the discrimination task requires discrimination of sign. The two methods yielded similar threshold functions (Figures 2a and 2b), providing evidence against the unlikely possibility that loss of sign applies to horizontal disparities. The second factor, increased noise near the horopter, may apply to horizontal disparities, but without support from measures other than threshold elevations, it is not an explanation. However, it is clear that the rising portion of the function in the data of McKee, Levi, and Bowne (1990) occurs at pedestals at which the stimulus is diplopic and the task becomes one of discriminating dichoptic width increments. For vertical disparities, then, the dip may mark the transition between disparity and width judgments, where thresholds drop as increments and decrements become discriminable as diplopia versus single vision. The same transition occurs with horizontal disparities of vertical lines, but there is no dip (McKee, Levi, and Bowne, 1990). The reason, perhaps, is that observers continue to use depth as a cue even above the horizontal diplopia threshold (Ogle, 1952, 1953).

Nonmonotonicities for horizontal disparity increments have appeared more robustly in model simulations than in empirical studies. Lehky and Sejnowski (1990) considered a population-code model based on the Poggio and Fischer (1977) three-channel disparity-coding scheme, containing broadly tuned "Near" and "Far" channels and a narrowly tuned near-horopter channel. Predicted increment thresholds from this model were sharply scalloped, with thresholds reaching their lowest values on either side of the horopter (their Figure 6b). This bore little resemblance to the target dataset, that of Badcock and Schor (1985), and the model was rejected; revised models containing larger sets of disparity channels were more successful (Lehky & Sejnowski, 1990). Tsai and Victor (2003) considered a multi-scale disparity-energy model, also with a population read-out, and reported a nearly flat but yet discernibly dipper-shaped increment threshold function when the model was reduced to contain only a single scale matched to the stimulus (their Figure 4d). This reduced version ought to approach the response of the full multi-scale model when the stimulus bandwidth is narrow and contrast is low, as in the case of the gratings used here. Finally, Zhao and Farell (2004) have shown that a disparity-energy model incorporating the full set of spatial frequency, orientation, and disparity sensitivities found in a V1 cortical column yields a dipper-shaped increment threshold function for grating stimuli. This outcome depended on a hierarchical read-out across disparity, orientation, and spatial frequency channels.

We simulated increment thresholds for our grating patterns using the Tsai and Victor (2003) and Zhao and Farell (2004) models. Both models compute phase-disparity energy (Ohzawa, DeAngelis, & Freeman, 1990). Figure 5 shows model thresholds plotted on linear axes on which minimal thresholds have been normalized to 1. The shapes of two model threshold functions bracket the range of observed shapes, though without corresponding precisely to any of them. Yet both models' threshold functions display a dip and their average is a good fit to the typical empirical function.

Tsai and Victor (2003) found that their model's response to 1.75-octave Gabor patterns approximated the exponential threshold functions observed empirically for comparable stimuli. For our grating patterns, the model shows a small dip centered on a pedestal of around 20° and a threshold range of about 1:1.6 over pedestals between 0° and 90°. Both results are quite robust across both stimulus

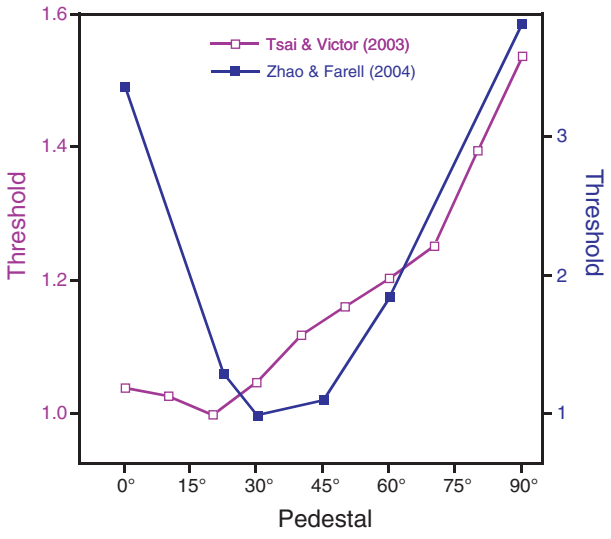

Figure 5. Disparity thresholds for sinusoidal gratings as function of disparity pedestal from the phase-disparity energy model of Tsai and Victor (2003) and Zhao and Farell (2004). For the former, gratings was 6 c/d and had a uniform contrast and a spatial extent that exceeded model receptive-field boundaries; for the later, grating was 1 c/d and had a contrast windowed by a 2-D Gaussian; model receptive fields tiled the stimulus. Threshold are plotted on linear scales with threshold minima normalized to unity.

and model parameters; the output seen in Figure 5 is typical of this model. Predicted thresholds are based on a mismatch function, an index of the neural response that cannot be accounted for by responses of template neurons. The shape of the mismatch function, measured as the reciprocal square root of the second derivative of this function at its minimum (Tsai & Victor, 2003), gives the smallest disparity increment that would be needed to overcome a specified amount of noise and so be detected; this is the threshold disparity increment shown, on arbitrary scaled units, in Figure 5. But in fact the model includes no sources of noise yielding trial-to-trial variation, so the details of the simulation results reflect deterministic model processes. The Zhao and Farell (2004) model has a front-end similar to that of Tsai and Victor's model, but has finer sampling of spatial frequency and disparity and includes filters tuned to all orientations. However, its pooling and decision processes are very different, being based primarily on a maximum-response rule rather than a population code. We believe it is primarily this latter difference that accounts for the variation between the models in the size and position of the dip and the range of the thresholds.

In both models the neurons' disparity-tuning functions form an envelope whose shape is a Gaussian centered at zero disparity (Tsai & Victor, 2003). The dip in the increment threshold function occurs approximately at the disparity where the gradient of these functions is steepest. This Gaussian gradient is specific to phase-disparity implementations of the models; a position-disparity implementation would have uniformly peaked tuning functions across the range of disparities covered and so no dip would be expected. The position of the dip will be affected not only by the shape and distribution of tuning functions but also by the pooling of neural responses at read-out. For multi-scale stimuli, a mixed set of gradients would contribute to the model's sensitivity at a particular disparity pedestal, and these scale differences in the gradients would wash out the dip.

In general, narrow bandwidth stimuli will produce a dip if the disparity channel with the sharpest tuning (relative to peak response) is centered on zero disparity, as in the Lehky and Sejnowski (1990) model, or if the maximum of the gradient of channel sensitivities is centered on zero disparity, as in phase-disparity energy models. Nonzero pedestals will then place the stimulus on the flanks of the central tuning curve, where it is steepest (McKee, Levi, & Bowne, 1990). Importantly, this does not require a broadening of channel tuning as the peak is displaced to larger disparities. So each channel can have the same bandwidth whether its preferred disparity is near the horopter or far from it (Qian & Zhu, 1997; Tsai & Victor, 2003; Zhao & Farell, 2004). An example is shown in Figure 6 for mechanisms with the same bandwidth and preferred spatial frequency that are sensitive to different but overlapping disparities, as found in the Tsai and Victor (2003) and Zhao and Farell (2004) models. These thresholded log-of-Gaussian tuning curves, c, are scaled vertically to have peak heights that trace out a Gaussian envelope, g, which appears in Figure 6 as the dashed line. Then the slope of the individual tuning curves is given by

$$\frac{dc}{d\delta} = k \times g(D) \times (D - \delta),$$

where δ is stimulus disparity, D is the disparity at the curve's peak, and k is a bandwidth-related constant. This shows that for each channel the slope is proportional to the height of that channel's peak. Thus channel slopes vary with disparity in proportion to the same Gaussian envelope in Figure 6 that's traced out by the channel peaks.

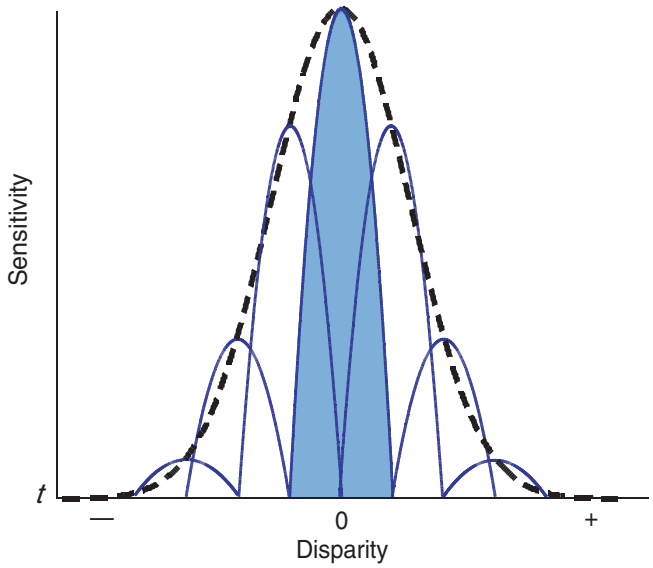

Figure 6. Tuning curves for mechanisms selective to disparity (blue lines) are shown as log-of-Gaussian functions, thresholded at *t*. Their peak sensitivities are greatest near the horopter, as shown here by the Gaussian envelope (black dashed line). For each of these tuning functions, the slope increases linearly with distance from the center disparity and has a value proportional to peak amplitude. Thus the most sensitive mechanism (shown as filled) also has the sharpest fall-off in sensitivity despite the equality of the bandwidths of all the mechanisms.

The steepest flanks fall on either side of the horopter, and it is here that sensitivity to disparity increments will be highest. Disparities closer to zero than this would be expected to produce a small drop in sensitivity; disparities farther from zero would lead to an accelerating drop in sensitivity, following the diminishing slope of the tuning functions. Qualitatively, this matches our data. A similar outcome would be expected for any envelope function that has its maximum at zero disparity and is monotonic on each side of zero.

The dip commonly found in contrast discrimination threshold functions (Nachmias & Kocher, 1970; Nachmias & Sansbury, 1974; Foley & Legge, 1981) has a related explanation in terms of an accelerating contrast response function (Nachmias & Kocher, 1970). However, note the

empirical difference: The contrast dip occurs at pedestals near the detection threshold, whereas the disparity dip occurs at pedestals exceeding stereo acuity by a factor of 3 or 4.

Stimulus bandwidth and the size-disparity correlation

The disparity thresholds measured here with narrow-bandwidth patterns typically show modest and non-monotonic variation over roughly half of the single-vision pedestal range (phase disparities of 0°-60°). The rather steep and monotonically increasing function typically reported for multi-scale patterns is readily derived from single-scale functions, even entirely flat single-scale functions, provided that disparity range and resolution co-vary with scale. The size-disparity correlation provides this linkage. Small pedestals place the left- and right-eyes' images within the disparity matching range of channels selective to the pattern's high-frequency components. Larger pedestals exceed this range and engage channels selective to lower frequencies. Spatial disparity thresholds will then increase with pedestal size, reflecting the decrease in resolution at coarser scales (Schor & Wood, 1983; Schor, Wood, & Ogawa, 1984a). Thus thresholds can be sampled at pedestal values for which increment thresholds are constant at any one scale and still contribute to an increasing function for multi-scale patterns, as sketched in Figure 7. The rate of increase would not necessarily be constant. Disparity thresholds for spatial frequencies greater than about 2 or 3 c/d, measured at zero pedestal, are usually found to be constant on a spatial scale (and so increase on a phase scale) (Schor, Wood, & Ogawa, 1984a). The effect would be a flattening of the increment threshold function at small pedestals, where thresholds are limited by responses to high-frequency components.

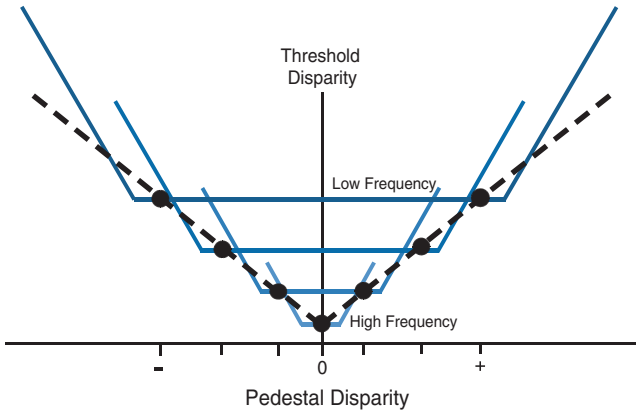

Figure 7. Increment threshold functions can be a flat function of disparity pedestal at any one scale (solid blue lines) and still contribute to an increasing function for multi-scale patterns (dashed black line). Dots depict sampling points for increment thresholds measured on a multi-scale stimulus. Increment thresholds for broadband patterns would increase over the range of pedestals mediated by components displaying constant threshold phase-disparity and a negative correlation between frequency and disparity range. A constancy of spatial disparities at high frequencies (Schor & Wood, 1983; Schor, Wood & Ogawa, 1984a) would flatten the broadband function at small disparities.

The size-disparity correlation assumes no interaction between channels of different scales in accounting for the rising increment threshold function. One can test this assumption by examining the effect of pattern bandwidth on stereo thresholds. Two studies, those of Smallman and MacLeod (1997) and Rohaly and Wilson (1993), compared increment thresholds for single-frequency and compound-frequency stimuli. In both cases the aim was to test for coarse-to-fine matching-range shifts (Marr & Poggio, 1979; Nishihara, 1984; Quam, 1987). The expectation was that these shifts would flatten the increment threshold function for compound stimuli, but flattening was not observed. Thresholds for two-frequency compounds were found to be roughly similar to those of the low-frequency component alone (Rohaly & Wilson, 1993) or to rise at an even faster rate with pedestal size (Smallman & MacLeod, 1997). These results imply that disparities of components of different scales are independently detected, perhaps with interference from finer scales as the size of the pedestal increases. Thresholds for multi-scale stimuli based on independent component detections would trace the lower envelope of the component thresholds, as seen in Figure 7, with allowances made for probability summation. A dip found at any one scale would contribute little to threshold functions sampled as coarsely as is typical for multi-scale patterns and scalloping of the function, as seen in Lehky and Sejnowski's (1990) initial simulation, would be smoothed by noise in any real threshold data.

Thus both the local detail (the dip) and the overall trend (a limited threshold range) that characterize the increment threshold function for the narrow bandwidth stimuli used here are consistent with extant models. The dip can be accounted for by models in which mechanisms tuned to disparity are most selective or most sensitive at a preferred disparity of zero. As just seen, these models are compatible also with a rapid rise in the threshold for broadband stimuli as pedestal size is increased.

Thus the observed features of the data are captured by multi-resolution models in which disparity channels operate independently of one another. The expectation, then, is that increment thresholds for broadband patterns should be approximately as steep as would be produced solely by means of independent disparity detection within channels tuned to different scales, as in Figure 7. We show in a subsequent report that this independence-based expectation is incorrect. It overestimates threshold at small-to-moderate pedestals and in some cases underestimates threshold at large pedestals (Farell, Li, & McKee, in press). The discrepancy is due to previously unobserved coarse-to-fine interactions among the components of multi-scale stimuli.

Acknowledgments

We wish to thank Dr. Jeffrey Tsai for use of the computer code for the Tsai and Victor model and for discussion of the model's operation. Supported by National Eye Institute Grants EY12286 to BF and EY06644 to SPM.

Commercial relationships: none.
Corresponding author: Bart Farell.
Address: Syracuse University, Institute for Sensory Research, Syracuse, NY, USA.
Email: bart_farell@isr.syr.edu.

Footnotes

1. An inability to compare a depth estimate with a memorized standard would not prevent an observer from performing the two-pedestal task, but it would explain the low performance level. Rather than comparing against a standard, the observer could compare depth estimates across successive trials, in effect treating successive trials as two intervals of a single trial. The difficulty of the task would then be understandable if depth judgments were ordinal, not metrical, for then between-trials comparisons would be productive on only a fraction of the trials. If depth order were judged separately for positive and negative disparities, the fraction is 50% (the fraction in which the stimulus on the previous trial had the same depth polarity); if depth order were judged on the basis of distance from observer without regard to sign of disparity, it is 37.5% (the fraction in which the stimulus on the previous trial had the same disparity or a larger disparity of the same sign). Remaining trials would require a guess, so the upper limit on performance would be 75% in the signed case and 68.75% in the unsigned case. Trial-by-trial analysis supports the former case. Observers can readily learn to use a single memorized depth standard (Morgan, Watamaniuk, & McKee, 2000); using two standards may be much more than twice as difficult. (If so, the effect might be specific to depth; the number of standards has only a small influence on discriminating separations in the fronto-parallel plane; Morgan, Watamaniuk, & McKee, 2000).

References

Andrews, T. J., Glennerster, A., & Parker, A. J. (2001). Stereo acuity thresholds in the presence of a reference surface. *Vision Research, 41*, 3051-3061. [PubMed]

Badcock, D. R., & Schor, C. M. (1985). Depth-increment detection function for individual spatial channels. *Journal of the Optical Society of America A, 2*, 1211-1216. [PubMed]

Blakemore, C. (1970). The range and scope of binocular depth discrimination in man. *Journal of Physiology, 211*, 599-622. [PubMed]

Brainard, D. H. (1997). The Psychophysics Toolbox. *Spatial Vision, 10*, 433-436. [PubMed]

Duwaer, A. L., & van den Brink, G. (1982). Detection of vertical disparities. *Vision Research, 22*, 467-478. [PubMed]

Erkelens, C. J., & Collewijn, H. (1985). Motion perception during dichoptic viewing of moving random-dot stereograms. *Vision Research, 25*, 583-588. [PubMed]

Farell, B. (1998). Two-dimensional matches from one-dimensional stimulus components in human stereopsis. *Nature, 395*, 689-693. [PubMed]

Farell, B. (2003). Detecting disparity in two-dimensional patterns. *Vision Research, 43*, 1009-1026. [PubMed]

Farell, B., Li, S., & McKee, S. P. (in press). Coarse scales, fine scales, and their interaction in stereo vision. *Journal of Vision*.

Felton, T. B., Richards, W., & Smith, R. A. Jr. (1972). Disparity processing of spatial frequencies in man. *Journal of Physiology, 25*, 349-362. [PubMed]

Fleet, D. J., Jepson, A. D., & Jenkin, M. R. M. (1991). Phase-based disparity measurement. *CYGIP: Image Understanding, 53*, 198-210.

Fleet, D. J., Wagner, H., & Heeger, D. J. (1996). Neural encoding of binocular disparity: Energy models, position shifts and phase shifts. *Vision Research, 36*, 1839-1857. [PubMed]

Foley, J. M., & Legge, G. E. (1981). Contrast detection and near-threshold discrimination in human vision. *Vision Research, 21*, 1041-53. [PubMed]

Harris, J. M., McKee, S. P., & Smallman, H. S. (1997). Fine-scale processing in human binocular stereopsis. *Journal of the Optical Society of America A, 14*, 1673-1683. [PubMed]

Hess, R. F., & Wilcox, L. M. (1994). Linear and non-linear filtering in stereopsis. *Vision Research, 34*, 2431-2438. [PubMed]

King-Smith, P. E., Grigsby, S. S., Vingrys, A. J., Benes, S. C., & Supowit, A. (1994). Efficient and unbiased modifications of the QUEST threshold method: Theory, simulations, experimental evaluation and practical implementation. *Vision Research, 34*, 885-912. [PubMed]

Krekling, S. (1974). Stereoscopic threshold within the stereoscopic range in central vision. *American Journal of Physiological Optics, 51*, 626-634. [PubMed]

Langley, K., Fleet, D. J., & Hibbard, P. B. (1999). Stereopsis from contrast envelopes. *Vision Research, 39*, 2313-2324. [PubMed]

Legge, G. E., & Gu, Y. (1989). Stereopsis and contrast. *Vision Research, 29*, 989-1004. [PubMed]

Lehky, S. R., & Sejnowski, T. J. (1990). Neural model of stereo acuity and depth interpolation based on a distributed representation of stereo disparity. *Journal of Neuroscience, 10*, 2281-2299. [PubMed]

Marr, D., & Poggio, T. (1979). A computational theory of human stereo vision. *Proceedings of the Royal Society of London, Series B, 204*, 301-328. [PubMed]

McKee, S. P., Levi, D. M., & Bowne, S. F. (1990). The imprecision of stereopsis. *Vision Research, 30*, 1763-1779. [PubMed]

McKee, S. P., Verghese, P., & Farell, B. (in press). What is the depth of a sinusoidal grating? *Journal of Vision*.

Morgan, M. J., Watamaniuk, S. N. J., & McKee, S. P. (2000). The use of an implicit standard for measuring discrimination thresholds. *Vision Research, 40*, 2341-2349. [PubMed]

Nachmias, J., & Kocher, E. C. (1970). Visual detection and discrimination of luminous increments. *Journal of the Optical Society of America, 60*, 382-389. [PubMed]

Nachmias, J., & Sansbury, R. V. (1974). Grating contrast: Discrimination may be better than detection. *Vision Research, 14*, 1039-1042. [PubMed]

Nishihara, H. K. (1984). Practical real-time imaging stereo matcher. *Optical Engineering, 23*, 536-545.

Ogle, K. N. (1952). On the limits of stereoscopic vision. *Journal of Experimental Psychology, 44*, 253-259. [PubMed]

Ogle, K. N. (1953). Precision and validity of stereoscopic depth perception from double images. *Journal of the Optical Society of America, 43*, 907-913. [PubMed]

Ohzawa, I., DeAngelis, G. C., & Freeman, R. D. (1990). Stereoscopic depth discrimination in the visual cortex: Neurons ideally suited as disparity detectors. *Science, 249*, 1037-1041. [PubMed]

Pelli, D. G. (1997). The VideoToolbox software for visual psychophysics: Transforming numbers into movies. *Spatial Vision, 10*, 437-442. [PubMed]

Pelli, D. G., & Zhang, L. (1991). Accurate control of contrast on microcomputer displays. *Vision Research, 31*, 1337-1350. [PubMed]

Poggio, G. F., & Fischer, B. (1977). Binocular interaction and depth sensitivity in striate and prestriate cortex of behaving rhesus monkey. *Journal of Neurophysiology, 40*, 1392-1405. [PubMed]

Qian, N., & Zhu, Y. (1997). Physiological computation of binocular disparity. *Vision Research, 37*, 1811-1827. [PubMed]

Quam, L. H. (1987). Hierarchical warp stereo. In M. A. Fischler & O. Firschein (Eds.), *Readings in computer vision* (pp. 80-86). Los Altos, CA: Kauffman.

Regan, D., & Beverley, K. I. (1973). Some dynamic features of depth perception. *Vision Research, 13*, 2369-2379. [PubMed]

Regan, D., Erkelens, J. C., & Collewijn, H. (1986). Necessary conditions for the perception of motion in depth. *Investigative Ophthalmology and Visual Science, 27*, 584-597. [PubMed]

Richards, W. (1971). Anomalous stereoscopic depth perception. *Journal of the Optical Society of America*, 61, 410-414. [PubMed]

Rohaly, A. M., & Wilson, H. R. (1993). Nature of coarse-to-fine constraints on binocular fusion. *Journal of the Optical Society of America A, 10*, 2433-2441. [PubMed]

Schor, C. M., & Badcock, D. R. (1985). A comparison of stereo and vernier acuity within spatial channels as a function of distance from fixation. *Vision Research, 25*, 1113-1119. [PubMed]

Schor, C. M., Edwards, M., & Pope, D. R. (1998). Spatial-frequency and contrast tuning of the transient-stereopsis system. *Vision Research, 38*, 3057-3068. [PubMed]

Schor, C. M., & Wood, I. (1983). Disparity range for local stereopsis as a function of luminance spatial frequency. *Vision Research, 23*, 1649-1654. [PubMed]

Schor, C. M., Wood, I. C., & Ogawa, J. (1984a). Spatial tuning of static and dynamic local stereopsis. *Vision Research, 24*, 573-578. [PubMed]

Schor, C. M., Wood, I., & Ogawa, J. (1984b). Binocular sensory fusion is limited by spatial resolution. *Vision Research, 24*, 661-665. [PubMed]

Schumer, R. A., & Julesz, B. (1984). Binocular disparity modulation sensitivity to disparities offset from the plane of fixation. *Vision Research, 24*, 533-542. [PubMed]

Siderov, J., & Harwerth, R. S. (1993a). Effects of the spatial frequency of test and reference stimuli on stereo-thresholds. *Vision Research, 33*, 1545-1551. [PubMed]

Siderov, J., & Harwerth, R. S. (1993b). Precision of stereoscopic depth perception from double images. *Vision Research, 33*, 1553-1560. [PubMed]

Siderov, J., & Harwerth, R. S. (1995). Stereopsis, spatial frequency and retinal eccentricity. *Vision Research, 35*, 2329-2337. [PubMed]

Smallman, H. S., & MacLeod, D. I. A. (1994). Size-disparity correlation in stereopsis at contrast threshold. *Journal of the Optical Society of America A, 11*, 2169-2183. [PubMed]

Smallman, H. S., & MacLeod, D. I. A. (1997). Spatial scale interactions in stereo sensitivity and the neural representation of binocular disparity. *Perception, 6*, 977-994. [PubMed]

Stelmach, L. B., & Buckthought, A. (2003). Pedestal depth discrimination for contrast modulated noise. *Journal of Vision, 3*, A460.

Tsai, J. J., & Victor, J. D. (2003). Reading a population code: A multi-scale neural model for representing binocular disparity. *Vision Research, 43*, 445-466. [PubMed]

Tyler, C. W. (1991). Cyclopean vision. In D. Regan (Ed.), *Vision and Visual Disorders* (pp. 38-74): Vol. 9. New York: Macmillan.

Watson, A. B., & Pelli, D. G. (1983). QUEST: A Bayesian adaptive psychometric method. *Perception and Psychophysics, 33*, 113-120. [PubMed]

Westheimer, G. (1979). Cooperative neural processes involved in stereoscopic acuity. *Experimental Brain Research, 36*, 585-597. [PubMed]

Westheimer, G., & McKee, S. P. (1978). Stereoscopic acuity for moving retinal images. *Journal of the Optical Society of America, 68*, 450-455. [PubMed]

Zhao, L., & Farell, B. (2004). The binocular neural mechanism: Disparity coding schemes, gnostic and population coding. Manuscript submitted for publication.